Research Article | Vol. 25, No. 24 | 27 Nov 2017 | OPTICS EXPRESS A1079

Optics EXPRESS

Determination of the absorption coefficient of chromophoric dissolved organic matter from underway spectrophotometry

GIORGIO DALL'OLMO,[1,2,*] ROBERT J. W. BREWIN,[1,2] FRANCESCO NENCIOLI,[1] EMANUELE ORGANELLI,[1] INA LEFERING,[3] DAVID MCKEE,[3] RÜDIGER RÖTTGERS,[4] CATHERINE MITCHELL,[5] EMMANUEL BOSS,[6] ANNICK BRICAUD,[7] AND GAVIN TILSTONE[1]

[1] *Plymouth Marine Laboratory, Prospect Place, Plymouth, PL1 3DH, UK*
[2] *National Centre for Earth Observations, UK*
[3] *Physics Department, University of Strathclyde, Glasgow, Scotland, UK*
[4] *Remote Sensing Department, Helmholtz-Zentrum Geesthacht, Geesthacht, Germany*
[5] *Bigelow Laboratory for Ocean Sciences, ME, USA*
[6] *University of Maine, Orono, ME, USA*
[7] *Sorbonne Universités, UPMC Univ Paris 06, CNRS, UMR 7093, Laboratoire d'Océanographie de Villefranche (LOV), 181 Chemin du Lazaret, 06230 Villefranche-sur-mer, France*
[*] *gdal@pml.ac.uk*

Abstract: Measurements of the absorption coefficient of chromophoric dissolved organic matter (a_y) are needed to validate existing ocean-color algorithms. In the surface open ocean, these measurements are challenging because of low a_y values. Yet, existing global datasets demonstrate that a_y could contribute between 30% to 50% of the total absorption budget in the 400-450 nm spectral range, thus making accurate measurement of a_y essential to constrain these uncertainties. In this study, we present a simple way of determining a_y using a commercially-available in-situ spectrophotometer operated in underway mode. The obtained a_y values were validated using independent collocated measurements. The method is simple to implement, can provide measurements with very high spatio-temporal resolution, and has an accuracy of about 0.0004 m^{-1} and a precision of about 0.0025 m^{-1} when compared to independent data (at 440 nm). The only limitation for using this method at sea is that it relies on the availability of relatively large volumes of ultrapure water. Despite this limitation, the method can deliver the a_y data needed for validating and assessing uncertainties in ocean-colour algorithms.

OCIS codes: (010.4450) Oceanic optics; (010.1030) Absorption.

References and links

1. C. D. Mobley, *Light and Water: Radiative Transfer in Natural Waters* (Academic Press, 1994).
2. A. Bricaud, M. Babin, H. Claustre, J. Ras, and F. Tieche, "Light absorption properties and absorption budget of southeast Pacific waters," J. Geophys. Res. **115**, C08009 (2010).
3. N. B. Nelson and D. A. Siegel, "The global distribution and dynamics of chromophoric dissolved organic matter," Annual Review of Marine Science **5**, 447–476 (2013).
4. E. Organelli, A. Bricaud, D. Antoine, and A. Matsuoka, "Seasonal dynamics of light absorption by chromophoric dissolved organic matter (CDOM) in the NW Mediterranean Sea (BOUSSOLE site)," Deep Sea Res. Part 1 **91**, 72–85 (2014).
5. A. Morel and B. Gentili, "A simple band ratio technique to quantify the colored dissolved and detrital organic material from ocean color remotely sensed data," Remote. Sens. Environ. **113**, 998–1011 (2009).
6. D. A. Siegel, S. Maritorena, N. B. Nelson, and M. J. Behrenfeld, "Independence and interdependencies among global ocean color properties: Reassessing the bio-optical assumption," J. Geophys. Res. **110**, C07011 (2005).
7. N. B. Nelson, D. A. Siegel, C. A. Carlson, C. Swan, W. M. Smethie, and S. Khatiwala, "Hydrography of chromophoric dissolved organic matter in the North Atlantic," Deep Sea Res. **54**, 710–731 (2007).
8. R. J. W. Brewin, G. Dall'Olmo, S. Pardo, V. van Dongen-Vogels, and E. S. Boss, "Underway spectrophotometry along the Atlantic Meridional Transect reveals high performance in satellite chlorophyll retrievals," Remote. Sens. Environ. **183**, 82–97 (2016).

#302375 https://doi.org/10.1364/OE.25.0A1079
Journal © 2017 Received 17 Jul 2017; revised 24 Oct 2017; accepted 24 Oct 2017; published 31 Oct 2017

Optics EXPRESS

9. G. Dall'Olmo, T. K. Westberry, M. J. Behrenfeld, E. Boss, and W. H. Slade, "Significant contribution of large particles to optical backscattering in the open ocean," Biogeosciences **6**, 947–967 (2009).
10. W. H. Slade, E. Boss, G. Dall'Olmo, M. R. Langner, J. Loftin, M. J. Behrenfeld, C. Roesler, and T. K. Westberry, "Underway and moored methods for improving accuracy in measurement of spectral particulate absorption and attenuation," J. Atmos. Ocean. Tech. **27**, 1733–1746 (2010).
11. T. K. Westberry, G. Dall'Olmo, E. Boss, M. J. Behrenfeld, and T. Moutin, "Coherence of particulate beam attenuation and backscattering coefficients in diverse open ocean environments," Opt. Express **18**, 15419–15425 (2010).
12. R. J. W. Brewin, G. Dall'Olmo, S. Sathyendranath, and N. J. Hardman-Mountford, "Particle backscattering as a function of chlorophyll and phytoplankton size structure in the open ocean," Opt. Express **20**, 17632–17652 (2012).
13. G. Dall'Olmo, E. Boss, M. Behrenfeld, and T. Westberry, "Particulate optical scattering coefficients along an Atlantic Meridional Transect," Opt. Express **20**, 21532–21551 (2012).
14. G. Dall'Olmo, E. Boss, M. J. Behrenfeld, T. K. Westberry, C. Courties, L. Prieur, M. Pujo-Pay, N. Hardman-Mountford, and T. Moutin, "Inferring phytoplankton carbon and eco-physiological rates from diel cycles of spectral particulate beam-attenuation coefficient," Biogeosciences **8**, 3423–3439 (2011).
15. P. J. Werdell, C. W. Proctor, E. Boss, T. Leeuw, and M. Ouhssain, "Underway sampling of marine inherent optical properties on the Tara Oceans expedition as a novel resource for ocean color satellite data product validation," Methods in Oceanography **7**, 40–51 (2013).
16. H. Claustre, F. Fell, K. Oubelkheir, L. Prieur, A. Sciandra, B. Gentili, and M. Babin, "Continuous monitoring of surface optical properties across a geostrophic front: Biogeochemical inferences," Limnol. Oceanogr. **45**, 309–321 (2000).
17. G. Kirkpatrick, C. Orrico, M. A. Moline, M. Oliver, and O. M. Schofield, "Continuous hyperspectral absorption measurements of colored dissolved organic material in aquatic systems," Appl. Opt. **42**, 6564–6568 (2003).
18. A. Matsuoka, E. Boss, M. Babin, L. Karp-Boss, M. Hafez, A. Chekalyuk, C.W. Proctor, P.J. Werdell, and A. Bricaud, "Pan-Arctic optical characteristics of colored dissolved organic matter: Tracing dissolved organic carbon in changing Arctic waters using satellite ocean color data," Remote. Sens. Environ. **200**, 89–101 (2017).
19. A. Bricaud, A. Morel, and L. Prieur, "Absorption by dissolved organic matter of the sea (yellow substance) in the UV and visible domains," Limnol. Oceanogr. **1**, 43–53 (1981).
20. J. M. Sullivan, M. S. Twardowski, J. R. V. Zaneveld, C. M. Moore, A. H. Barnard, P. L. Donaghay, and B. Rhoades, "Hyperspectral temperature and salt dependencies of absorption by water and heavy water in the 400-750 nm spectral range," Appl. Optics **45**, 5294–5309 (2006).
21. W. S. Pegau, D. Gray, and J. R. V. Zaneveld, "Absorption and attenuation of visible and near-infrared light in water: dependence on temperature and salinity," Appl. Optics **36**, 6035–6046 (1997).
22. R. Röttgers, D. McKee, and C. Utschig, "Temperature and salinity correction coefficients for light absorption by water in the visible to infrared spectral region," Opt. Express **22**, 25093–25108 (2014).
23. E. Boss, W. H. Slade, M. Behrenfeld, and G. Dall'Olmo, "Acceptance angle effects on the beam attenuation in the ocean," Opt. Express **17**, 1535–1550 (2009).
24. X. Zhang, L. Hu, and M.-X. He, "Scattering by pure seawater: Effect of salinity," Opt. Express **17**, 5698–5710 (2009).
25. M. S. Twardowski, E. Boss, J. M. Sullivan, and P. L. Donaghay, "Modeling the spectral shape of absorption by chromophoric dissolved organic matter," Mar. Chem. **89**, 69–88 (2004).
26. R. F. Davis, C. C. Moore, J. R. V. Zaneveld, and J. M. Napp, "Reducing the effects of fouling on chlorophyll estimates derived from long-term deployments of optical instruments," J. Geophys. Res. Oceans **102**, 5851–5855 (1997).
27. E. S. Boss, R. Collier, G. Larson, K. Fennel, and W. S. Pegau, "Measurements of spectral optical properties and their relation to biogeochemical variables and processes in Crater Lake, Crater Lake National Park, OR," Hydrobiologia **574**, 149–159 (2007).
28. I. Lefering, R. Röttgers, C. Utschig, and D. McKee, "Uncertainty budgets for liquid waveguide CDOM absorption measurements," Appl. Optics **56**, 6357–6366 (2017).
29. P. Kowalczuk, G. H. Tilstone, M. Zablocka, R. Röttgers, and R. Thomas, "Composition of dissolved organic matter along an Atlantic Meridional Transect from fluorescence spectroscopy and Parallel Factor Analysis," Mar. Chem. **157**, 170 – 184 (2013).
30. P. G. Coble, "Marine optical biogeochemistry: The chemistry of ocean color," Chem. Rev. **107**, 402–418 (2007).
31. A. Morel, "Are the empirical relationships describing the bio-optical properties of case 1 waters consistent and internally compatible?" J. Geophys. Res. Oceans **114**, C01016 (2009).
32. V. Kitidis, A. P. Stubbins, G. Uher, R. C. U. Goddard, C. S. Law, and E. M. S. Woodward, "Variability of chromophoric organic matter in surface waters of the Atlantic Ocean," Deep Sea Res. Part 2 **53**, 1666 – 1684 (2006).
33. R. M. Pope and E. S. Fry, "Absorption spectrum (380-700 nm) of pure water. 2. Integrating cavity measurements," Appl. Optics **36**, 8710–8723 (1997).
34. A. Bricaud, A. Morel, M. Babin, K. Allali, and H. Claustre, "Variations of light absorption by suspended particles with chlorophyll a concentration in oceanic (Case 1) waters: Analysis and implications for bio-optical models," J. Geophys. Res. Oceans **103**, 31033–31044 (1998).
35. A. Bricaud, H. Claustre, J. Ras, and K. Oubelkheir, "Natural variability of phytoplanktonic absorption in oceanic waters: influence of the size structure of algal populations," J. Geophys. Res. Oceans **109**, C11010 (2004).
36. A. Bricaud, A. M. Ciotti, and B. Gentili, "Spatial-temporal variations in phytoplankton size and colored detrital matter absorption at global and regional scales, as derived from twelve years of SeaWiFS data (1998-2009)," Global.

Biogeochem. Cycles **26**, GB1010 (2012).
37. R. J. W. Brewin, D. E. Raitsos, G. Dall'Olmo, N. Zarokanellos, T. Jackson, M. F. Racault, E. S. Boss, S. Sathyendranath, B. H. Jones, and I. Hoteit, "Regional ocean-colour chlorophyll algorithms for the Red Sea," Remote. Sens. Environ. **165**, 64–85 (2015).

1. Introduction

Chromophoric dissolved organic matter (CDOM, also known as yellow substance or "gelbstoff") is one of the optically-significant constituents found in natural waters [1]. Recent estimates from a global dataset suggest that, in the surface open ocean, CDOM contributes on average approximately 50% of the total absorption at 440 nm [2–4] and thus interferes with retrievals of chlorophyll-a concentration from space (chl [5, 6]). Therefore, accurate measurements of CDOM absorption (a_y) are critical to both validating existing and to developing novel ocean-colour algorithms. Yet, a_y measurements in the surface open ocean remain relatively are sparse, due to the difficulties in measuring its characteristically low values in the visible spectral range. To overcome this limitation, long-pathlength capillary waveguides are typically employed with single-beam spectrophotometers, but this method is time consuming [2, 7].

Chlorophyll concentrations (chl) spectrophotometrically determined by an underway WETLabs ACS instrument were recently used to validate satellite ocean-colour data [8]. The underway system consisted of an optical set up that sampled seawater pumped through the ship's clean seawater supply [8]. This study demonstrated that semi-automatic measurements can result in considerably lower uncertainties than traditional methods, because they avoid errors related to human intervention. Following these encouraging results for chl and others for the particulate absorption, attenuation and backscattering coefficients [9–15], the current study focused on developing and validating a semi-automated method for determining a_y using an underway ACS instrument that sampled surface open-ocean waters.

Other studies have attempted to estimate surface a_y from continuous measurements. Surface underway optical properties including estimates of a_y using a WETLabs AC9 meter were collected in the Alboran Sea, but unfortunately these estimates were not directly validated, due to lack of independent measurements [16]. A liquid waveguide capillary cell (LWCC) was deployed in automated mode to estimate a_y and compared favourably with discrete a_y estimates determined with a benchtop spectrophotometer [17]. More recently, continuous underway 0.2-μm filtered absorption coefficients were determined with a WETLabs ACS meter during the Tara-Arctic cruise and were calibrated by means of discrete a_y estimates from a LWCC system [18]. Despite these previous efforts, estimating a_y in continuous underway mode remains a relatively uncommon method. The present work is an attempt to demonstrate that continuous underway spectrophotometric measurements can be reliably exploited to estimate a_y with very high spatio-temporal resolution.

1.1. Measurement principle

To determine a_y using an ACS instrument (or any other in-situ spectrophotometer) in a flow-through system, the principle used in the laboratory can be employed: a_y is obtained by subtracting from the absorption coefficient of 0.2-μm filtered seawater ($a_{0.2}$) the absorption coefficient of ultrapure water (a_{MQ}).

The above simple subtraction, however, always produces data, that in the spectral region above 550 nm, differ significantly from the expected exponentially-decreasing a_y spectra [19]. To understand these differences, when using the absorption channel (a) of the ACS instrument, it is useful to explicitly write the components of $a_{0.2}$ and a_{MQ} (the wavelength dependency is omitted for simplicity):

$$a_{0.2} = a_\Delta + a_w + a_{b_w} + a_{b_{salt}} + \Psi_T T_{0.2} + \Psi_S S + a_y, \tag{1}$$

Optics EXPRESS

$$a_{\mathrm{MQ}} = a_{\Delta} + a_w + a_{b_w} + \Psi_T T_{\mathrm{MQ}}, \tag{2}$$

here a_{Δ} is the bias due to any drift in the calibration coefficients of the absorption meter; a_w is the absorption coefficient of pure water; a_{b_w} is the (spurious) absorption signal due to the scattering of pure water that is not collected by the reflecting tube of the ACS [20]; $a_{b_{salt}}$ is the (spurious) absorption signal due to the scattering induced by dissolved salts; Ψ_T and Ψ_S are the temperature- and salinity-dependence coefficients of pure-water absorption, respectively [20–22]; $T_{0.2}$ and T_{MQ} are the temperatures of the 0.2-μm filtered seawater and ultrapure water, respectively; and S is the salinity of the 0.2-μm filtered seawater.

Data collected by the attenuation channel (c) of the ACS can also be exploited to independently determine the absorption of dissolved substances, if we assume that CDOM does not scatter light significantly. In this case the following equations are used:

$$c_{0.2} = c_{\Delta} + a_w + b_w + b_{salt} + \Psi_T T_{0.2} + \Psi_S S + c_y, \tag{3}$$

$$c_{\mathrm{MQ}} = c_{\Delta} + a_w + b_w + \Psi_T T_{\mathrm{MQ}}, \tag{4}$$

where c_{Δ} is the bias due to any drift in the calibration coefficients of the attenuation meter; b_w is the scattering of pure water (accounting for the acceptance angle of the transmissometer, [23]); b_{salt} is the scattering of dissolved salts; and c_y is the estimate of CDOM attenuation (in general, Ψ_T and Ψ_S are different for a and c [20], but, for simplicity, we here ignore these differences). Under the above assumption, a_y and c_y should be equal. However, throughout this work we will use the two symbols to distinguish the estimates obtained from the two ACS channels. Finally, for simplicity, we here omit including the effect caused by the change in refractive index with salinity at the instrument optical window [20] and assume this is negligible in our case.

By subtracting the signal of the ultrapure water from that of 0.2-μm filtered seawater we obtain the following quantities:

$$a_{0.2} - a_{\mathrm{MQ}} = a_y + a_{b_{salt}} + \Psi_T (T_{0.2} - T_{\mathrm{MQ}}) + \Psi_S S, \tag{5}$$

$$c_{0.2} - c_{\mathrm{MQ}} = c_y + b_{salt} + \Psi_T (T_{0.2} - T_{\mathrm{MQ}}) + \Psi_S S. \tag{6}$$

Thus, the spectrum resulting from subtracting the absorption (or attenuation) spectrum of ultrapure water from that of 0.2-μm filtered seawater contains information on a_y or c_y (henceforth $[a, c]_y$), but is also affected by the spectral features of Ψ_T, Ψ_S, of $a_{b_{salt}}$ and b_{salt}. Importantly, note how the a_{MQ} and c_{MQ} spectra are used to remove instrumental drifts, which otherwise would contribute to make the pure-water spectra significantly different from zero.

The spectral features introduced by Ψ_T can range between 0.001 and 0.01 m^{-1} at 600 nm and between 0.01 and 0.1 m^{-1} at 740 nm for $T_{0.2} - T_{\mathrm{MQ}}$ ranging between 1 and 10 degrees C [20, 22] (these $T_{0.2} - T_{\mathrm{MQ}}$ values are similar to those found in this study). Features due to Ψ_S for typical salinity values of 35 are of the order of 0.0014 and 0.014 m^{-1} at 600 and 730 nm, respectively [20, 22]. However, both Ψ_T and Ψ_S show significant spectral features only above approximately 550 nm [20, 22]. Since a_y increases exponentially towards the blue spectral region, the temperature and salinity dependence of pure water do not interfere significantly with the spectrum of $a_{0.2} - a_{\mathrm{MQ}}$ between 400 and 550 nm.

On the other hand, $a_{b_{salt}}$ and b_{salt} also increase exponentially towards the blue spectral region, but their expected typical values amount to approximately 0.001 m^{-1} at 440 nm [24]. Thus, correcting for errors introduced by the scattering of salts is important only for extremely small values of a_y.

Optics EXPRESS

2. Material and methods

2.0.1. Field campaign

Data were collected during the 26th Atlantic Meridional Transect (AMT26), which took place on board the RRS James Clark Ross from September 20th (Immingham, UK) to November 4th, 2016 (Port Stanley, Falkland Islands). The transect spanned approximately 100 degrees of latitude and covered a wide range of oceanic waters ranging from oligotrophic to eutrophic (Fig. 1).

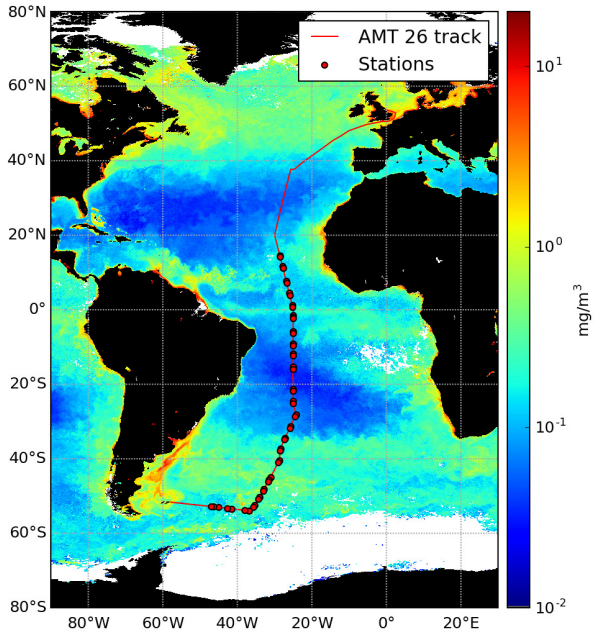

Fig. 1. AMT26 track (line) and locations of discrete validation samples (circles) superimposed onto the October 2016 Ocean Colour-ESA Climate Change Initiative (v3.1) monthly chl composite.

2.0.2. Experimental set up

The set up used to collect measurements is similar to the one described in previous work [9, 13] and exploits a WETLabs hyperspectral (400-750 nm) absorption and attenuation meter (ACS) that continuously samples water from the ship's clean seawater supply. Every hour, for ten minutes, an automated electrically-actuated valve diverts the sample water through a 0.2-μm cartridge filter (Cole Parmer, single open end serial nylon cartridge, 0.45/0.20 μm). The 0.2-μm filtered signals are subtracted from the bulk data to derive calibration-independent particulate absorption (a_p) and beam attenuation (c_p) coefficients. To derive a_p and c_p a simultaneous scattering and residual temperature correction is applied [9, 10].

2.0.3. Measurements needed to determine a_y

To derive $[a, c]_y$, we determined the absorption and attenuation coefficients of 0.2-μm filtered water from the ship's clean seawater supply as well as those of the ship's ultrapure water system (Millipore Milli-Q_{185} Plus reagent-grade water purification system equipped with UV photo-oxidation technology that was fed with water pre-treated by reverse osmosis; final resistivity: 18.2 MΩ cm^{-1}; total organic carbon $\leq$5 ppb). To account for variations in the instrument calibration coefficients, four ultrapure water measurements, at intervals of approximately 6 hours, were

collected each day during the cruise. This ultrapure water was contained in an acid-washed 20 l carboy and pumped to the ACS by means of positive pressure applied to the carboy. To remove any remaining particles in the ultrapure water, an additional 0.2-μm filter (AcroPack, 1000 capsule with Supor membrane, 0.2/0.2 μm) was installed between the carboy and the ACS. Measurements were collected as the ultrapure water flowed through the ACS for about 5 minutes. Each ultrapure water measurement was taken just after one of the automated 0.2-μm filtrations so that quasi-simultaneous data on 0.2-μm filtered seawater were available.

2.0.4. Estimation of "discrete" a_y and c_y values

The measurements provide two spectra for the both a- and c-channels: one set when the ACS tubes are filled with 0.2-μm filtered seawater, i.e. $[a, c]_{0.2}$, and one set when filled with ultrapure water, i.e. $[a, c]_{\mathrm{MQ}}$. To estimate $[a, c]_y$, we first computed the difference between the measured absorption and attenuation coefficients of the 0.2-μm filtered and ultrapure water:

$$[a, c]_{\mathrm{y,raw}} = [a, c]_{0.2} - [a, c]_{\mathrm{MQ}}. \tag{7}$$

Note that we did not apply the temperature and salinity corrections recommended by the manufacturer, because CDOM absorbs in the blue spectral region where these corrections have relatively small spectral variations [20].

Finally, we fitted a single exponential curve with an offset [25] using a non-linear optimization routine [25] to $[a, c]_{\mathrm{y,raw}}$ in the 420-490 nm region:

$$[a, c]_y(\lambda) = \left([a, c]_{\mathrm{y,raw}}(440)\right) e^{S_y(440-\lambda)} + O, \tag{8}$$

where S_y is the spectral slope and λ is the wavelength (in nm), and O is an offset (in m^{-1}). The fitting region was chosen to minimise interferences from Ψ_T and to avoid wavelengths shorter than 420 nm where the ACS intrinsic noise increases. A randomly-selected example of this fit is presented in Fig. 2. Since we did not apply any temperature and salinity corrections, large spectral features are evident in the $[a, c]_{\mathrm{y,raw}}$ spectrum above 490 nm (black line in Fig. 2). On the other hand, in the blue spectral region the spectrum follows the typical exponentially decreasing shape of a_y .

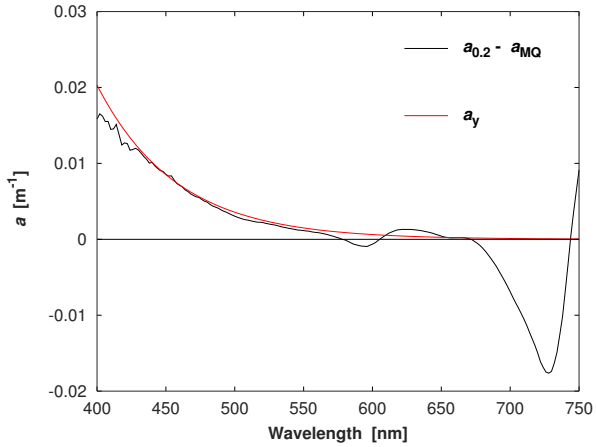

Fig. 2. Example of fitting eq. 8 to the difference between the absorption coefficients of 0.2-μm filtered and ultrapure water in the 430-490 nm spectral range. The local minima and maximum in the $a_{0.2} - a_{\mathrm{MQ}}$ spectrum at wavelengths longer than 550 nm are due to temperature and salinity differences between the two water samples.

Optics EXPRESS

2.1. Estimation of "hourly" a_y and c_y values

After deriving $[a, c]_y$ from discrete daily measurements of ultrapure water, we also estimated hourly values of $[a, c]_y$ by interpolating the four daily ultrapure water measurements to match the hourly values of 0.2-μm filtered seawater. The main assumption here is that the diurnal variability of the ultrapure water signal measured by the ACS can be approximated by linearly interpolating successive ultrapure water measurements.

To obtain hourly 0.2-μm filtered water measurements we computed the median value of spectra collected during the central part of the hourly 0.2-μm filtration time (from minute 2 to minute 9 of every hour). Finally, we computed hourly estimates of $[a, c]_{y,\mathrm{raw}}$ and estimated hourly spectra of $[a, c]_y$ as described in the previous section.

2.2. How many ultrapure water measurements do we need?

An important practical methodological question is: How often is a ultrapure water spectrum (and related experiment) needed during any given cruise? While the answer may depend on how stable the specific ACS instrument used is, we carried out a sensitivity analysis to calculate how the uncertainty in the ultrapure water value increases with a decrease in the number of ultrapure water samples available.

To provide an estimate of how the temporal resolution of the MQ measurements could affect the uncertainties in the derived $[a, c]_y$ values, we estimated the standard deviation of the $[a, c]_{\mathrm{MQ}}$ signal during each day of the cruise. Results from this calculation provide an estimate of the typical variability of the MQ signal (and thus of the stability of the ACS instrument) during a single day. To estimate how stable the ACS was during sets of two days, we then increased the interval within which we computed the standard deviation to 2 consecutive days and repeated the calculation. We finally repeated the process, by increasing the intervals by 1 day until we reached a final interval of 7 consecutive days.

2.3. Estimation of chlorophyll-a concentration

To compare our $[a, c]_y$ measurements with published bio-optical models, we estimated the concentration of chlorophyll-a (chl) by exploiting the peak in a_p at 676 nm [9, 26, 27]. This calculation assumes a chlorophyll-specific absorption coefficient that is constant [9, 26, 27]. We compared these ACS-based estimates of chl with independent and coincident determinations of total chlorophyll-a (TChla, sum of chl-a, divinyl chl-a, and chlorophyllide-a) from high performance liquid chromatography (from discrete samples filtered on glass fiber filters, with filtered volumes ranging between 2 and 5 litres based on the trophic status of the sampled waters). The median of the relative residuals (chl/TChla-1) was -0.15, and their robust standard deviation was 0.08, indicating that the ACS-based estimates of chl were typically underestimating TChla by about 15% and had a typical precision of about 8%. To remove this bias from our ACS-based estimates of chl, we therefore multiplied them by a factor 1.15 and used these corrected values for the rest of the analysis.

To obtain chl matching the a_y spectra, we first removed high-frequency variability by applying a median filter (window size 171) to the minute-binned chl values. The hourly gaps in chl during the 0.2-μm filtration times were then filled by linear interpolation of the median-filtered values. Finally, hourly chl values were extracted to match in time the $[a, c]_y$ values.

2.4. Validation

To validate our ACS-based estimates of $[a, c]_y$, we collected additional independent measurements using a liquid waveguide capillary cell (LWCC) system.

Water samples were collected from the CTD Niskin bottles and the underway system in 0.1-l acid-washed amber glass bottles. To minimize possible temperature artefacts in the measurements,

Optics EXPRESS

the samples and reference waters (see below) were kept in a water bath at room temperature between collection and analysis. CTD samples were collected twice a day (before dawn and at noon) from 5-m depth (corresponding to the nominal depth of the intake of the underway system). Underway samples were generally collected twice a day, at the time of the noon CTD cast and in the evening.

All samples were analyzed on-board within few hours with a spectrophotometric system that included: a liquid waveguide capillary cell (3000 series, World Precision Instruments, with a calibrated optical pathlength of 98.71 cm); a deuterium-halogen light source (DH-2000-BAL), a spectrometer and two optical fibers (USB 2000+, Ocean Optics Inc., FL, USA) connecting the light source to the waveguide cell and the waveguide cell to the spectrometer. To minimize measurements artefacts due to changes in system geometry, all system components were fixed to the work bench in the same configuration for the entire duration of the campaign. Reliable measurements were obtained from about 20° N to 55° S (Fig. 1).

The spectrometer software generated absorbance spectra (A, wavelength dependency omitted) from 350 to 750 nm. A is defined as

$$A = \log_{10}\left(\frac{I_R}{I_S}\right) \tag{9}$$

where I_R and I_S are the radiant power spectra transmitted through reference water and sample water, respectively. To allow the software generating A spectra, I_R was estimated once a day measuring ultrapure water. Furthermore, to track drifts in the lamps, ultrapure water measurements were collected before and after each sample of solution measured (see below). Neither the "boxcar smoothing" nor the "electronic dark" options on the Ocean Optics software were used.

The measured A spectra were converted into absorption spectra (a) as follows:

$$a = \frac{2.303A}{d} \tag{10}$$

where d is the optical pathlength of the LWCC and the factor 2.303 is used to convert from logarithm in base 10 to natural logarithm.

The system lamps were switched on at least one hour before each daily cycle of analysis, to ensure adequate warm up and stability. Each day, before the analysis, the capillary waveguide was cleaned by injecting a 10% vol/vol HCl acid solution followed by a 50% methanol solution with a 10-ml syringe [2]. It was then rinsed by 3 injections of ultrapure water. The LWCC was also rinsed with ultrapure water at the end of each day. No detergent (e.g., Decon) was used, because it increased the chances of introducing bubbles in the LWCC. To minimize contamination, ultrapure water used for the baseline and to track any drift in the baseline (reference) was stored in 0.1-L amber glass bottles, and kept separate from the ultrapure water used for rinsing.

The optical quality of the ultrapure water produced by the ship's Millipore system was verified on a daily basis by comparing it with HPLC-grade water (Fisher Scientific, product number W/0120/PB15) at the beginning and at the end of each cycle of analysis. No significant differences were found between the ultrapure water and the HPLC-grade water.

Rinsing ultrapure water, reference ultrapure water and seawater samples were injected in the LWCC using 10-ml plastic syringes on which 0.2-μm filters (30 mm, Spartan, hydrophilic regenerated cellulose membrane, Whatman) were mounted. To minimize contamination, we used separate syringes and filters for rinsing, reference, and samples. Before each cycle of analysis, all syringes were cleaned with the HCl and methanol solutions, and then rinsed 3 times with ultrapure water. All filters were rinsed 5 times with 10 ml of ultrapure water. After injection, to minimize artefacts due to variations in pressure inside the waveguide, the syringe was disconnected from the LWCC before a spectrum was recorded. Readings were then taken quickly to minimise temperature changes of the sample due to light-induced heating. Particular attention was paid

during each injection to minimize the formation of bubbles within the LWCC, because they affect the transmission of light through the sample and can lead to an overestimation in absorbance. More specifically, 1) we avoided the use of detergents, which significantly increased the rate of bubble appearance; 2) after acid and methanol cleaning, the system was rinsed multiple times with ultrapure water until all bubbles present (especially near tubing connections) were removed; 3) before injecting the samples, two or three ultrapure water injections were used to confirm that the spectra were stable and reproducible (indicating that no bubbles were present); 4) before connecting the syringe and filter to the injection tubing, some sample drops were expelled from the syringe over the end of the injection tubing, to ensure that this tubing was completely full of liquid; 5) all samples were injected through 0.2-μm filters.

For each seawater sample we acquired measurements from 3 replicate injections. Syringe and filter were flushed with each sample before the first injection. For each injection, 20 spectra were recorded at a frequency of roughly 1 Hz (each spectrum the average of ~50 scans collected every 20 ms), and then averaged together. This averaging was needed, because the system showed significant sensitivity to ship rolling in the visible portion of the spectrum (spectra shifted in the visible range, but not in the UV range, depending on the roll angle of the ship, most likely due to variations of the visible light source). Reference ultrapure water spectra were collected before and after each seawater sample to track (and correct for) drifts in the baseline. Between samples, sample syringe and filter were rinsed 3 times with 10 ml of ultrapure water.

LWCC measurements are affected by the salinity of the sample that changes the transmissivity through the capillary in addition to the change in water absorption [7,28]. To obtain a_y spectra, we thus needed to account for this effect by using a solution of NaCl in ultrapure water as a blank. A NaCl solution at 36 psu was produced each day using 100 ml of ultrapure water and 3.6 g of NaCl (weighed before the cruise and stored in ashed glass vials; Extra Pure, SLR, Fisher Chemical, product code S/3120/53), previously combusted at 450°C for 4 hours. Spectra of 0.2-μm filtered NaCl-solution were collected at the beginning and at the end of each day. As for the seawater samples, reference ultrapure water spectra were collected before and after each NaCl-solution measurement to track (and correct for) drifts in the baseline.

Unfortunately, every time we determined the absorption spectrum of the NaCl solution, variations were observed during the 20 replicate measurements that were collected for each NaCl-solution sample, which may be due to impurities in the salt. Specifically, after injecting the NaCl solution, an absorbance peak rapidly developed between 350 and 450 nm during the typical 20 seconds needed to collect the 20 spectra. Simultaneously, the absorbance of the NaCl solution gradually decreased below 300 nm, potentially suggesting that a photochemical reaction was taking place as the NaCl solution was exposed to the UV-visible light. This effect was never observed when we measured natural seawater samples, ultrapure or HPLC-grade water. Thus, to perform salinity corrections, we could not use the average of the 20 spectra as was done for the samples, ultrapure and HPLC-grade water. Instead, we were forced to use the very first spectrum collected immediately after the injection of the NaCl solution. This first spectrum was minimally affected by the peak between 350 and 450 nm.

To verify that this first NaCl-solution spectrum was minimally affected by the artefact peak between 350 and 450 nm, and therefore that the salt corrections were accurate, a second series of NaCl-solution spectra was acquired post-cruise. This time, a higher purity NaCl (Honeywell Fluka puriss. p.a. ACS Reagent, ≥99.5%, product code: 31434-1KG-R) was used to produce a series of solutions with salinity varying from 31 to 45 psu with a 2 psu interval. The resulting spectra were not affected by the artefact peak observed during the field experiment. Consistently with previous results [7], these spectra also showed that absorbance has only a modest dependency on salinity over the salinity-range used. While absorbance values were lower than those observed at sea by a constant offset at all wavelengths (likely due to difference in the system geometry related to the new set up), the overall shape of the spectra was qualitatively similar. Thus, we

concluded that the (very first) NaCl-solution spectra collected at sea were sufficiently accurate to apply the salt correction.

Before computing a_y, all spectra were smoothed with a Gaussian moving average (6 nm width), to remove high-frequency spectral oscillations due to the interference patterns generated by salt-induced variations in refraction within the LWCC [28].

Finally, a_y was derived as:

$$a_y = \left(a_{\text{sample}} - a_{\text{MQ}}\right) - \left(a_{\text{NaCl}} - a^*_{\text{MQ}}\right), \tag{11}$$

where a_{sample}, a_{MQ}, a_{NaCl}, a^*_{MQ} are the absorption spectra measured for the sample, the reference ultrapure water of the sample, the NaCl solution and the reference ultrapure water of the NaCl solution, respectively.

3. Results

3.1. MQ water measurements

Figure 3 shows that the absorption and attenuation values measured during all ultrapure water experiments conducted during the cruise drifted significantly with respect to the values recorded at the beginning of the cruise. In addition, the drifts of the absorption and attenuation signals were different and displayed step changes when the instrument was turned off and cleaned. These drifts and step changes clearly demonstrate the need to collect multiple ultrapure water measurements during the cruise to obtain the instrument baselines needed to estimate $[a, c]_y$.

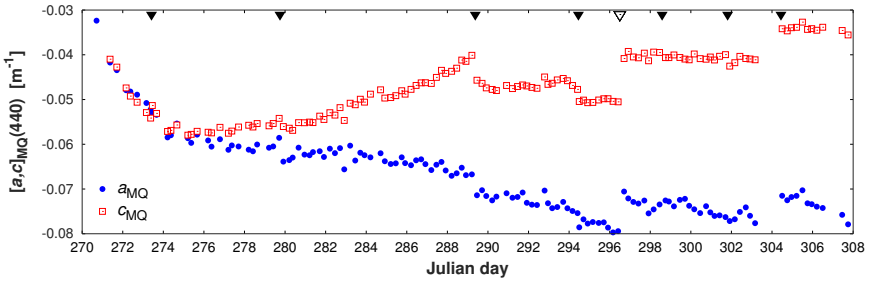

Fig. 3. Absorption (blue circles) and attenuation (red empty squares) coefficients of ultrapure water as measured during the course of the cruise. Black and white triangles indicate times when the ACS instruments was cleaned and when it was switched off for about 2 hrs, respectively.

Furthermore, the typical uncertainty of this baseline increases with the time interval between ultrapure water measurements (Fig. 4). These data suggest that to achieve measurements of $[a, c]_{\text{MQ}}$ within ± 0.002 m^{-1}, at least one ultrapure water measurement per day would be required, provided that measurements are also collected before and after the instrument is cleaned or restarted.

3.2. All $[a, c]_y$ spectra

Discrete $[a, c]_{y,\text{raw}}$ spectra showed strong spectral features at wavelengths longer than about 490 nm due to differences in temperature and salinity between the 0.2-μm filtered water and the ultrapure water (Fig. 5, top plots). However, as expected, at wavelengths shorter than 490 nm, $[a, c]_{y,\text{raw}}$ spectra showed the typical exponential increase towards shorter wavelengths [19]. $a_{y,\text{raw}}$ and $c_{y,\text{raw}}$ spectra were remarkably similar below 490 nm, confirming that either channel of the ACS can be used to derive CDOM absorption in this spectral range. However, residuals

Optics EXPRESS

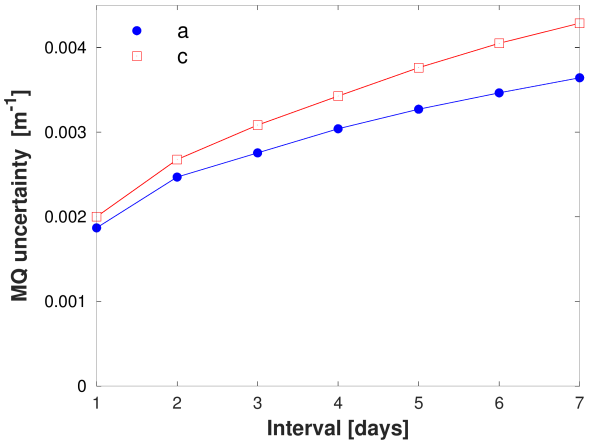

Fig. 4. Estimated typical uncertainties in $[a, c]_{\mathrm{MQ}}(440)$ as a function of the temporal resolution at which ultrapure water measurements are collected. Each point in the figure represents the average of all the standard deviations computed on subsets of the $[a, c]_{\mathrm{MQ}}(440)$ time series. These subsets were obtained by subdividing the time series in intervals of varying length as reported on the x-axis.

from the fits in the 420-490 nm range of $[a, c]_{y,\mathrm{raw}}$ were smaller for the c-tube than for the a-tube of our ACS (Fig. 5).

3.3. Validation

The comparison between $[a, c]_y(440)$ derived from the ACS and the $a_y(440)$ independently estimated with the LWCC is presented in Fig. 6. The main results are those obtained for the LWCC data corrected using the salinity values determined during the cruise (left plot in Fig. 6), because this salinity correction was derived using the same instrumental set up used to measure a_y. These results show that our ACS-based estimates were in good agreement with the LWCC measurements with typical biases (i.e., median of residuals) smaller than about 0.0004 m^{-1} and precisions (i.e., robust standard deviation of residuals) of about ± 0.0030 m^{-1} . In relative terms, these correspond to a median bias of about <1% and a precision of ±22%, for the observed a_y (440) range (0.005-0.02 m^{-1}).

Results from the LWCC processed using the laboratory-obtained salinity coefficients are also presented (right plot in Fig. 6) to demonstrate the effect of the salinity correction on the precision of this comparison (the larger biases in the right plot are due to differences in instrument set up [28]). Specifically, this second comparison demonstrates that the cluster of points at low values of $[a, c]_y(440)$ (i.e., LWCC cruise sal < 0.005 m^{-1}) disappears when the laboratory-based salinity correction is applied and it is thus due to uncertainties in the salinity correction obtained during the cruise, rather than in the ACS estimates. Future studies should ensure that salinity corrections in the field are obtained using NaCl with minimal amounts of impurities.

Most of the LWCC samples (i.e., 70%) were collected from Niskin bottles. The agreement observed between the $[a, c]_y$ estimated by ACS using water from the ship's underway system and the LWCC samples collected from the rosette also demonstrates that the ship's seawater supply was not biasing the measured CDOM absorption coefficients.

3.4. Differences between a_y and c_y

Consistently with the comparison given in Fig. 6, our estimates of a_y and c_y at 440 nm were in relatively good agreement, with a small bias of -0.0002 m^{-1} and a typical spread of their

Optics EXPRESS

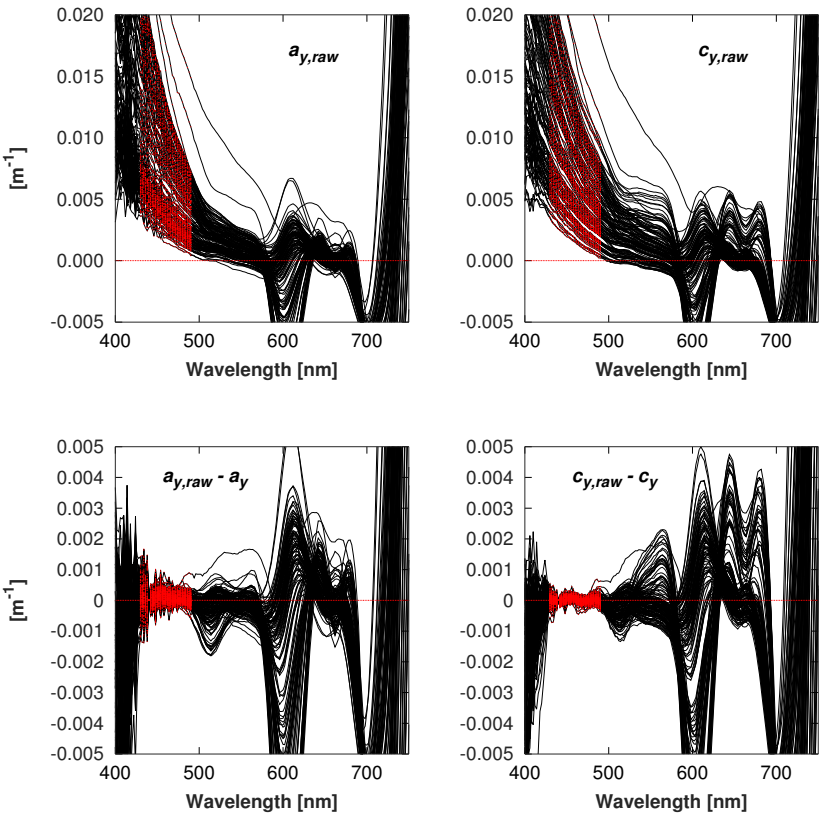

Fig. 5. Top: $[a, c]_{y,\mathrm{raw}}$ spectra measured during AMT26 (black); red dots indicates the spectral range used to fit eq. 8. Bottom: residuals from the fit of eq. 8 to the $[a, c]_{y,\mathrm{raw}}$ spectra. Red lines highlight the zero values.

differences of about 0.0021 m^{-1} (Fig. 7). However, these differences varied systematically during the course of the cruise, with more negative values at the beginning of the cruise and more positive values at the end (Fig. 7). No correlation was found between these differences and other variables such as sea surface temperature and salinity or chlorophyll concentration (not shown). It thus remains unclear what could explain these small, but systematic deviations.

3.5. Spatial variability of $a_y(440)$ and chl

The absorption coefficient of CDOM at 440 nm showed spatial variations that were, in general, positively correlated with variations in chl and that reflect the different water masses and trophic regimes encountered during the Atlantic Meridional Transect (Fig. 8). Specifically, $a_y(440)$ values were highest at high latitudes, intermediate near the equatorial upwelling region and minimal in the subtropical gyres (Fig. 8, [29]). The relatively large variability surrounding the relationship between chl and $a_y(440)$, particularly between 0.3 and 0.8 mg m^{-3}, suggest that CDOM dynamics are also controlled by processes different from those controlling phytoplankton pigments [3, 4, 19, 30].

The estimated $a_y(440)$ values were positively correlated with chl, although a relatively large

Optics EXPRESS

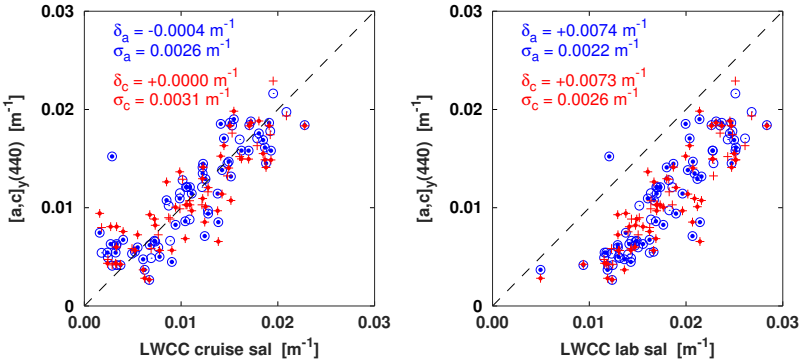

Fig. 6. Comparison between $[a, c]_y(440)$ measured by the ACS and by the LWCC. Two different sets of LWCC data are shown: (left) data processed by applying the salinity correction determined during the cruise and (right) in the laboratory. Blue circles and text refer to a_y estimates, red crosess and text to c_y estimates. Filled circles are comparisons for which the LWCC samples were collected from the Niskin bottles, rather than from the ship's seawater supply. δ values are the median absolute residuals (LWCC - ACS) and are used as an indicator of the bias. σ values are the robust standard deviations of the debiased residuals (i.e., residuals from which the corresponding δ was subtracted) computed as the half differences between the 84^{th} and 16^{th} percentiles and are used as a robust indicator of the spread of these residuals (σ corresponds to the standard deviation, if the distribution is normal). Both metrics were computed using the entire dataset. δ and σ are used as indicators of accuracy and precision. Dashed lines represent the 1:1 relationship.

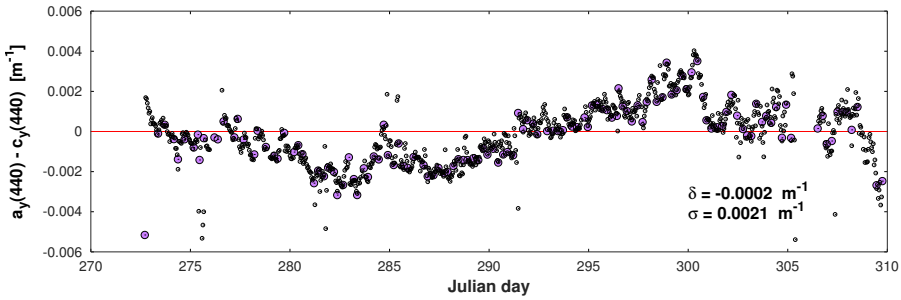

Fig. 7. Time series of the differences between a_y and c_y at 440 nm during the cruise. Large and small circles represent discrete and hourly estimates, respectively. Median (δ) and robust standard deviations (σ) of the differences are also presented.

scatter is observed (Fig. 9). Our estimates are also relatively consistent with previously published bio-optical models [2, 31, 32], although at the high range of chl, our $a_y(440)$ estimates were significantly lower than those predicted by these models. The following regression equation was obtained by fitting the AMT26 dataset:

$$a_y(440) = 0.0179\ chl^{\,0.438}, \quad (N = 822, R^2 = 0.49). \tag{12}$$

3.6. Contribution of a_y to total absorption

The variability in the contribution of a_y to the total absorption coefficient at 440 nm is presented in Fig. 10. To compute $a_{tot}(440)$ we employed the pure water absorption coefficient

Optics EXPRESS

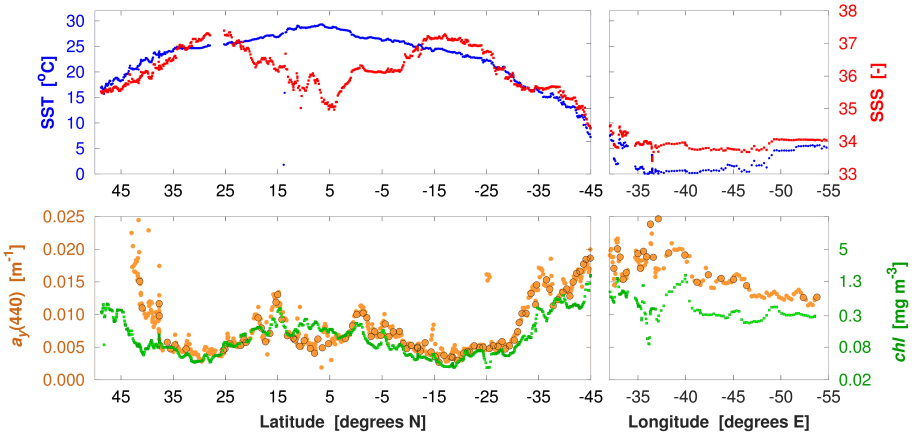

Fig. 8. Spatial variability of sea surface temperature (SST), salinity (SSS), $a_y(440)$ and chlorophyll concentration (chl). Large and small orange circles in bottom plots indicate $a_y(440)$ estimates for which ultrapure water measurements were available ("discrete") and for which the absorption by ultrapure water was interpolated ("hourly"), respectively.

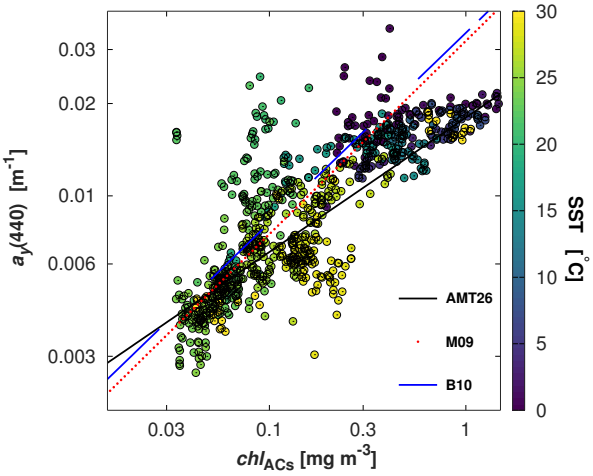

Fig. 9. Scatterplot of hourly $a_y(440)$ vs. chl with colors representing sea surface temperature. The black line represents the bio-optical model derived from the AMT26 dataset. Blue dashed line and dotted line represent bio-optical models relating chl to a_y ("M09" for [31], "B10" for [2]).

determined at 440 nm by [33]. These results suggest that on average (± 1 standard deviation) $a_y(440) : a_{tot}(440) = 0.32 \pm 0.11$ and that, during the AMT, this ratio varied the most (i.e., 0.2 – 0.6) for chl ranging between 0.05 and 0.3 mg m^{-3}. Our average $a_y(440) : a_{tot}(440)$ vs. chl relationship are generally consistent with published bio-optical models, except perhaps at the highest chl we observed [2, 34, 35].

Optics EXPRESS

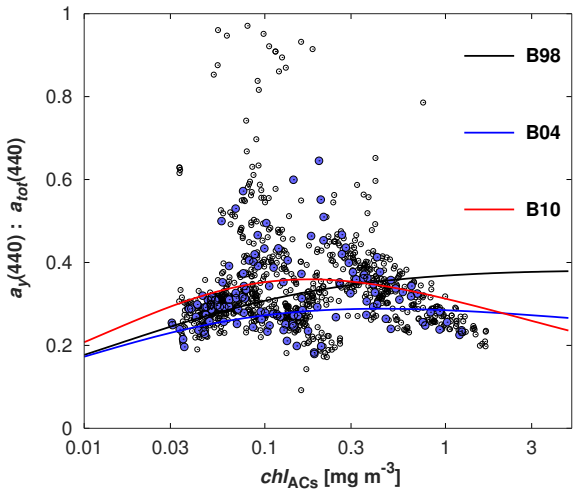

Fig. 10. Relative contribution of a_y to the total absorption coefficient (a_{tot}) at 440 nm as a function of chl. Large filled and small empty circles were derived by using discrete and hourly estimates of a_y, respectively, and coincident measurements of $a_p(440)$. The black, blue, and red lines were derived from previously published relationships for a_y [2], pure water absorption [33] and for three different models of a_p [2, 34, 35], respectively.

3.7. *Spectral slope vs.* $[a, c]_y(440)$

The spectral slopes of $[a, c]_y$ followed the expected general trend of decreasing slopes at higher $[a, c]_y$ values and compared favourably with published bio-optical models [36, 37] (Fig. 11). The relatively large slope values at low $[a, c]_y$ are likely due to the narrow range used for fitting the data. In addition, a cluster of points with $a_y(440)$ values larger than about 0.012 m^{-1} was also characterised by anomalously high spectral slopes. These points belonged to the part of the transect south of approximately 35°S characterised by cold sea surface temperatures and potentially suggest that these water masses could have had CDOM absorption coefficients with different spectral characteristics.

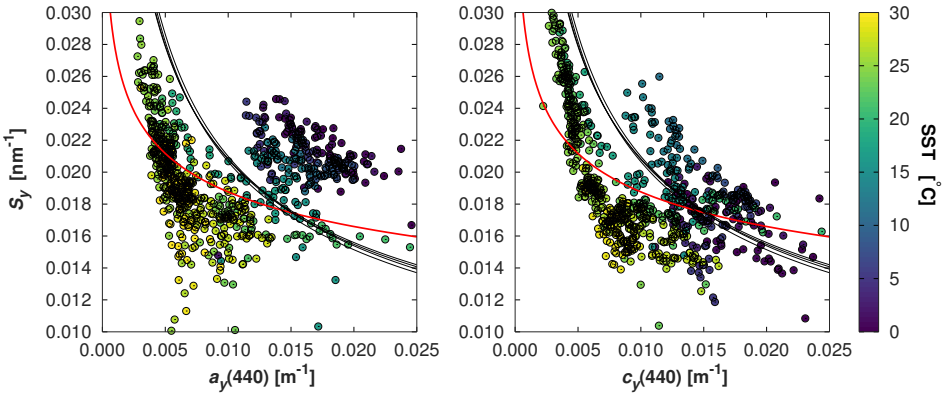

Fig. 11. Scatterplots of $[a, c]_y(440)$ vs. the spectral slope of CDOM absorption fitted between 440 and 550 nm. Color represents sea surface temperatures. Black and red lines are published bio-optical models [36, 37].

Optics EXPRESS

4. Discussion

In this study, we have demonstrated how to estimate the absorption coefficient of CDOM using a WETLabs ACS spectrophotometer operated in an underway system. We have also demonstrated that these underway a_y estimates are consistent with independent discrete estimates collected by the LWCC system and with existing bio-optical models.

4.1. Advantages

This new way of operating the ACS instrument has advantages over traditional methods for measuring a_y in the surface open ocean.

First, the ACS appears to be sensitive enough to measure the low values of a_y we sampled in the oligotrophic parts of the AMT26 (~0.005 m^{-1} at 440 nm). This is due to the relatively long pathlength (25 cm) of this instrument, to the availability of quasi-simultaneous determinations of the instrument baseline, provided by the ultrapure water measurements, and to the relatively large temporal averaging.

Second, two independent estimates of the CDOM absorption coefficients are obtained (one from the absorption channel of the ACS and one from the attenuation channel), which can be used to assess the uncertainty in the method and potentially could be averaged to increase its precision. When compared to independent LWCC estimates, these estimates are accurate to within about 0.0004 m^{-1} and have a precision of about 0.0025 m^{-1} (Fig. 6), although the reported precision also depends on the LWCC uncertainties [28].

Third, the method is very simple to implement: it only requires one to collect regular measurements of ultrapure water during the course of the field campaign. Also the data processing is relatively simple, as it only requires to fit eq. 8 to the difference between the absorption by 0.2-μm filtered seawater and that of ultrapure water, thus avoiding the need for temperature and salinity corrections of the absorption data.

Finally, by interpolating the regular ultrapure water spectra to each of the 0.2-μm filtration times, quasi-continuous (hourly, in this study) estimates of CDOM absorption can be derived. Of course, by increasing the frequency of the 0.2-μm filtrations, the spatio-temporal resolution of the a_y estimates can be also increased.

4.2. Disadvantages

The main disadvantage of this method is that it requires relatively large volumes of ultrapure water to determine the drift in the instrument baseline. Although the volume used for determining each ultrapure water absorption could be reduced from the 20 l we used in this study, to rinse and fill the flow cell of the ACS an amount of ultrapure water considerably larger (order of a liter) than that used for the LWCC method (order of few ml) would be needed. In addition, because of the increased risk of contamination, uncertainties could increase if the volume of ultrapure water was reduced. Practically, large volumes of ultrapure water can only be obtained if a reliable purification system is available on the ship where the optical underway system is operated.

An additional limitation is that the wavelength range is constrained (in this study from 420 to 490 nm) by the spectral resolution of the ACS meter, its sensitivity that decreases at wavelengths shorter than about 450 nm, and the need to avoid absorption features related to the temperature and salinity dependencies of pure water. While the latter features can potentially be removed [10], this additional processing step may result in little scientific gain, because most of the open-ocean CDOM absorption is in the blue region. We therefore opted for a simpler method that can be easily applied, but is restricted to a smaller spectral range.

Finally, although the ACS sensitivity appeared to be sufficient for the waters sampled during the AMT26 transect, it is possible that, in waters with smaller amounts of CDOM, the 25-cm pathlength may not be long enough to determine a_y. In such cases, the instrumental precision

Optics EXPRESS

could be increased by averaging over longer sampling times.

4.3. Recommendations

The following recommendations are provided for potential future users of this method:

- Verify the optical purity of the ultrapure water by comparing it to a standard (e.g., HPLC-grade pure water), because ships' purification systems may be operating in non-ideal conditions.
- Tune the frequency of ultrapure water measurements to the required uncertainty in a_y.
- Ensure that ultrapure measurements are collected before and after the ACS is powered off or cleaned, to minimize step changes in the baseline values.
- Verify the cleanliness of the ship's seawater supply for each cruise, because seawater pumped by the ship could be biased with respect to the surface ocean waters. To this aim, estimates of a_y need to be compared to collocated measurements of a_y determined on water collected from the ship's rosette. In this study, we conducted these additional measurements using a LWCC system. However, in principle, this comparison could be conducted using the ACS, as long as enough water from the rosette is available.

5. Conclusions

We have presented a simple method to derive estimates of the CDOM absorption coefficient in the surface open ocean using a spectrophotometer operated in underway mode. The method allows one to collect measurements with very high spatio-temporal resolution. If the recommended protocols are followed, the resulting data could be added to growing number of underway optical measurements that are used to validate ocean-colour sensors.

Funding

European Space Agency (ESA) (ESRIN/RFQ/3-14457/16/I-BG); National Atmospheric and Space Administration (NASA) (NNX14AP86G).

Acknowledgments

The authors would like to thank the captain, chief scientist, officers and crew of the RRS James Clark Ross for the help they provided during the AMT26 field expedition. The authors would like to acknowledge one anonymous reviewer for their constructive comments that helped improve a draft version of this paper. This study is a contribution to the international IMBeR project and was supported by the UK Natural Environment Research Council National Capability funding to Plymouth Marine Laboratory and the National Oceanography Centre, Southampton. This is contribution number 315 of the AMT programme. This study was supported by the European Space Agency contract: Copernicus Sentinel Atlantic Meridional Transect Fiducial Reference Measurements Campaign (AMT4SentinelFRM). EB contribution was supported by NASA's OBB program. Support from the UK National Centre for Earth Observation is also acknowledged.